Astron. Astrophys. 324, 1135–1144 (1997)

ASTRONOMY
AND
ASTROPHYSICS

The photon dominated regions associated with NGC 2023 and S 140

F. Wyrowski[1], **C.M. Walmsley**[1,2], **A. Natta**[2], **and A.G.G.M. Tielens**[3]

[1] I. Physikalisches Institut, Univ. zu Köln, Zülpicherstr. 77, D-50937 Köln, Germany
[2] Osservatorio Astrofisico di Arcetri, Largo E.Fermi 5, I-50125 Firenze, Italy
[3] NASA Ames Research Center, MS 245-3, Moffet Field, CA 94035, USA

Received 24 September 1996 / Accepted 21 February 1996

Abstract. We have used the Effelsberg 100-m telescope to observe the C91α radio recombination line towards the photon-dominated regions associated with NGC 2023 and S 140. This has been supplemented with observations of the $C^{18}O$ (2-1) and (3-2) lines using the 3-m KOSMA telescope. We have analyzed the C91α observations using 1-dimensional homogeneous models in order to derive estimates of the density and ultraviolet radiation field. Towards both sources, our radio line data suggest densities of 10^5 cm^{-3} although we have evidence for a drop-off to a value of around 10^4 cm^{-3} at offsets of 0.4 pc from the exciting star in NGC 2023. The molecular line data towards NGC 2023 are also consistent with high densities (certainly above 10^4 and probably of order 10^5 cm^{-3}). We discuss the influence of clumping on these models and conclude that densities as high as 10^6 cm^{-3} are possible in both the molecular and carbon line emitting gas.

Key words: ISM: clouds – ISM: molecules – radio lines: ISM – ISM: NGC 2023; S 140

1. Introduction

One of the interesting developments of the past few years has been the increase in our understanding of the structure of the interface regions between HII regions and molecular clouds. Such interfaces are commonly called "Photon Dominated Regions" or PDRs. The increase in understanding is partly due to the relative ease to observe the FIR fine structure lines which are mainly responsible for cooling PDRs. The [C II] fine structure transition at 158 μm is perhaps the best tracer of PDRs . A discussion of the characteristics of this transition is given in the review article of Genzel (1992). Detailed 1-dim. models of PDR structure have been computed by Tielens & Hollenbach (1985).

In this paper we consider the intensity ratio of the carbon radio recombination lines and the FIR carbon fine structure line. This ratio turns out to be density sensitive as discussed by Natta et al. (1994) who used the Effelsberg 100-m to make observations of C91α at 3 cm towards Orion and compared the measured intensity with measurements of the [C II] 158 μm line by Stacey et al. (1993). The basic point made by Natta et al. was that at the densities of importance in Orion, the [C II] 158 μm intensity is roughly proportional to the C^+ column density as long as the [C II] 158 μm optical depth is low, whereas the radio recombination line intensity is proportional to the carbon emission measure ($\int N_e N(C^+) ds$). The consequence is that the ratio of their intensities is approximately proportional to density. The detailed calculations of Natta et al. show that this statement only holds up to densities of about 10^6 cm^{-3}. At higher densities, heating by collisional deexcitation of vibrational states of H_2 becomes increasingly effective and causes a temperature rise which reduces the intensity of the radio line. But at lower densities, the ratio of the radio and FIR line intensities is a reasonable density estimator.

One of the interesting results from the Natta et al. study was the detection of the carbon radio line at relatively large distances from the source of UV radiation. The C91α line was found 1 pc in projected distance to the east of the Trapezium stars at a position where the radiation field was roughly a factor of 500 lower than, for example, towards the star Θ^1C responsible for most of the ionization. This suggested it would be useful to observe C91α towards other sources where measurements of the [C II] 158 μm line are available and where the UV radiation field is expected to be moderate. We therefore carried out C91α measurements towards the sources NGC 2023 and S 140 using the Effelsberg 100-m telescope.

The reflection nebula NGC 2023 is a site where a cluster of young pre main-sequence stars has been detected in the L 1630 cloud (E. Lada et al. 1991). The main source of ultraviolet photons is thought to be the B1.5 star HD 37903 (Harvey et al. 1980) although a more highly reddened object , "star C" (Sellgren et al. 1992 and references therein) may be important in the southern part of the region. HD 37903 has a visual extinction of only 1.4 magnitudes and is thought to be situated near the front side of L 1630. The visual scattered light distribution is well fit by a spherical model centered on HD 37903 with a dust

Send offprint requests to: F. Wyrowski

free cavity of size 25″ (Witt et al. 1984). This corresponds to 0.05 pc at a distance of 415 pc (Anthony-Twarog 1982).

Carbon recombination lines were detected from the region by Knapp et al. (1975) and studied at higher angular resolution by Pankonin & Walmsley (1976, 1978). They were interpreted as being due to the combination of a core of dimensions roughly 0.15 pc and a halo whose size is thought to be an order of magnitude larger. The [C II] 158 μm line emission has been mapped with an angular resolution of approximately 1′ (Jaffe et al. 1990, Howe et al. 1991, Jaffe et al. 1994). Their maps show a structure centered just to the south of HD 37903 with a dimension of roughly 0.3 pc. Higher angular resolution views of the PDR have been obtained in the molecular hydrogen v=1-0 S(1) line by Gatley et al. (1987) and Field et al. (1994). Burton et al. (1992) showed that the H_2 emission is in large part due to fluorescence and that it is spatially correlated with 8727 A [C I] emission which (see Natta et al. and references therein) is thought to be produced in the same region as the radio lines. Burton et al. estimated densities above 10^5 cm^{-3} in this C^+ layer and Fuente et al. (1995) derived similar values for the adjacent molecular region from their CN data.

S 140 is a small bright HII region on the south-west border of the molecular cloud L 1204. It is excited by the B0 star HD 211880 located to the south-west of the ionized rim. To the north-east (about 1′ or 0.3 pc offset at a distance of 900 pc) is a small group of embedded infrared sources which form a strong FIR source with a luminosity of $2 \cdot 10^4$ L$_\odot$(Harvey et al. 1978). S 140 has also been the subject of intensive study in molecular lines (Blair et al. 1978, Ungerechts et al. 1986, Zhou et al. 1993, Zhou et al. 1994) and atomic fine structure transitions (Keene et al. 1985, Boreiko et al. 1990, Hernichel et al. 1992). C166α and C141α emission was found by Knapp et al. (1976) towards the infrared source with angular resolutions of 22.5′ and 21′ respectively. Recently, Smirnov et al. (1995) have measured C166α at three positions with 9′ resolution but to our knowledge there has not been work done at higher frequencies. Schneider et al. (1995) have recently mapped the [C II] 158 μm line towards S 140 at 55″ angular resolution and this prompted us to observe C91α towards this source.

In this paper, we present a C91α map of NGC 2023 and measurements of this transition towards two positions in S 140. We supplement the radio recombination line data with a map of $C^{18}O$ (2-1) and (3-2) towards NGC 2023 using the 3-m KOSMA telescope. We have estimated physical parameters in both the molecular and photon-dominated regions and compare the two. Sect. 2 outlines our observational techniques and Sect. 3 summarizes the main observational results. In Sect. 4, we consider a variety of models aimed at allowing estimates of the physical parameters in the NGC 2023 PDR. In Sect. 5, we summarize very briefly our estimates for the density and ultraviolet radiation field in S 140. Sect. 6 is devoted to the characteristics of the molecular gas in NGC 2023 and Sect. 7 summarizes our conclusions.

2. Observations

2.1. C91α observations of NGC 2023 and S 140

The observations were carried out using the Effelsberg 100-m telescope on November 7 and 8 1994. The half-power beamwidth at this frequency is 82″. Pointing was checked through observations on NGC 7027 and 3C 161 at roughly hourly intervals and has an accuracy of 5″. The receiver was the facility dual-channel HEMT with a receiver temperature of 70-80 K. The observing mode was frequency switching with a throw of 1.5 MHz symmetrically with respect to the line frequency. The spectrometer was an autocorrelator which was split into two sections of 512 channels and centered on the C91α (8589.104 MHz) and the H91α line (8584.821 MHz). A bandwidth of 2.5 MHz was used yielding a spectral resolution of 0.2 km s^{-1}.

2.2. $C^{18}O$ observations of NGC 2023

We mapped $C^{18}O$ (2-1) and (3-2) towards NGC 2023 using the 3-m KOSMA telescope (see Winnewisser et al. 1990) on Gornergrat in conjunction with the Cologne dual channel SIS receiver system. The half-power beamwidths of the telescope at the frequencies of $C^{18}O$ (2-1) (219560.333 MHz) and $C^{18}O$ (3-2) (329330.505 MHz) are 115 and 75″, respectively. Pointing was checked on Venus and was found to be accurate within 30″. We observed in position switching mode with a reference position at (-15′, 0′) offset from HD 37903.

The receivers were operated in double sideband mode and calibration was carried out using the normal chopper calibration technique. In the case of $C^{18}O$ (3-2) this is somewhat inaccurate due to the presence of the strong nearby atmospheric water absorption which causes the image band opacity to be considerably different from that in the signal band (the intermediate frequency is 1.5 GHz). We have corrected for this using the model atmosphere of Grossman (1989) and estimate our error to be 15% in both lines by comparing the line intensities at the offset (0, -1′) from day to day. We used the facility acousto-optic spectrometers with spectral resolutions of 0.2 and 0.6 km s^{-1} and bandwidths of 287 and 1388 MHz at 220 and 330 GHz respectively.

In order to check for high optical depth in the $C^{18}O$ emission, we also measured $C^{17}O$ (2-1) (224714.371 MHz) and (3-2) (337061.096 MHz) at 12 positions around the offset (0,-1′). For this transition, the calibration of the (3-2) data is less sensitive to the atmospheric water line.

3. Observational results

In the case of NGC 2023, the line intensities were sufficiently strong that we were able to make a small map whereas towards S 140, our observations were confined to two positions. The central position of our NGC 2023 map was the position of the star HD 37903 ($\alpha(1950) = 05^h39^m07\overset{s}{.}3$, $\delta(1950) = -02^\circ16'58''$) and offsets given later in this paper are relative to this position. The two positions measured

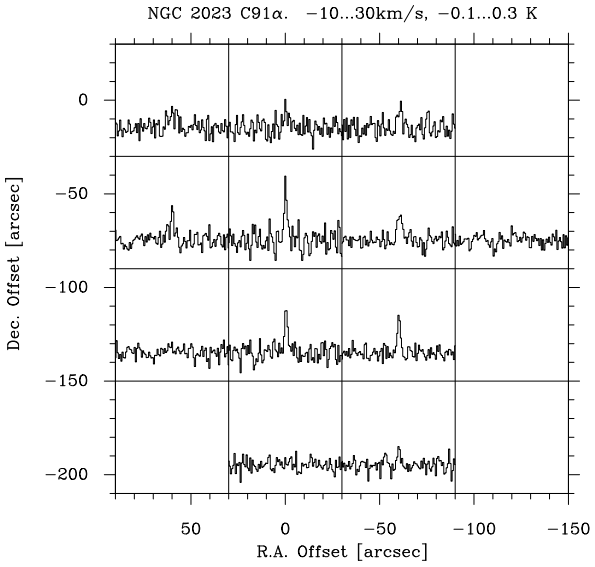

Fig. 1. C91α lines detected in NGC 2023. Abscissa is LSR velocity from -10 to 30 km s^{-1} and ordinate is line temperature from -0.1 to 0.3 K.

Table 1. Line parameters derived from Gaussian fits of C91α.

Source	Offsets ($''$)	$T_{\rm MB}$ (K)	$V_{\rm LSR}$ (km s^{-1})	$\Delta v_{1/2}$ (km s^{-1})
NGC2023	(60, 0)	0.05 ± 0.02	10.3 ± 0.4	3.7 ± 0.6
	(60, -60)	0.09 ± 0.02	9.9 ± 0.2	2.4 ± 0.5
	(60,-120)	< 0.02		
	(0, 0)	0.06 ± 0.03	10.3 ± 0.3	2.1 ± 0.8
	(0, -60)	0.21 ± 0.03	10.1 ± 0.8	1.2 ± 0.2
	(0,-120)	0.16 ± 0.03	10.3 ± 0.8	1.2 ± 0.2
	(0,-180)	< 0.04		
	(-60, -60)	0.09 ± 0.02	10.5 ± 0.1	2.1 ± 0.3
	(-60,-120)	0.14 ± 0.02	10.1 ± 0.1	1.2 ± 0.2
	(-60,-180)	0.07 ± 0.02	10.1 ± 0.1	1.1 ± 0.4
	(-120, -60)	< 0.04		
	(-60, 0)	0.08 ± 0.03	10.5 ± 0.2	1.8 ± 0.6
S140	(-60, -60)	0.03 ± 0.01	-7.2 ± 0.5	5 ± 1
	(0, 0)	0.05 ± 0.01	-7.4 ± 0.2	3.2 ± 0.4

in S 140 were towards the embedded IR sources (α(1950) = $22^h17^m41\overset{s}{.}1$, δ(1950) = 63°03′42″) and towards the ionization front (α(1950) = $22^h17^m37\overset{s}{.}1$, δ(1950) = 63°02′42″). We give in Table 1 the line parameters determined from Gaussian fits and in Figs. 1 and 2 we show the corresponding spectra.

3.1. C91α towards NGC 2023

Fig. 3 shows a contour map of the integrated C91α intensity towards NGC 2023 (solid lines). The emission peaks at the position (1″, -81″) relative to HD 37903 and in declination the angular half-power width which we measure is 136″ or 108″ (0.22 pc) if we correct for a beamsize of 82″ assuming a Gaussian source distribution. One can compare this with the

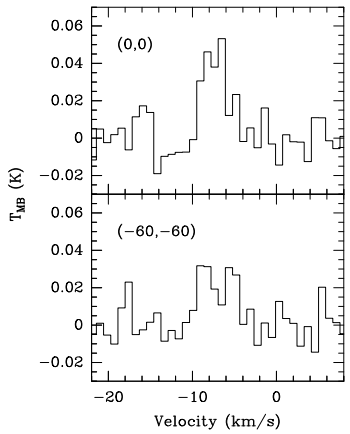

Fig. 2. C91α lines detected in S 140. (0,0) is the position of IRS 1 and (-60″,-60″) is a position on the ionization front.

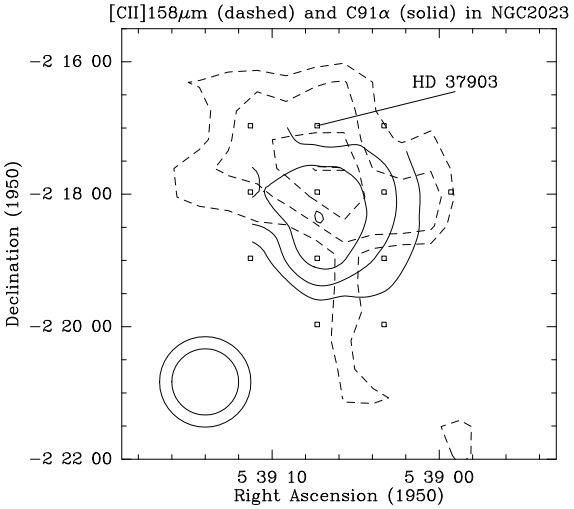

Fig. 3. Integrated intensity maps of the radio recombination line C91α (solid) and of the [C II] 158 μm far infrared line (dashed, taken from Jaffe et al. 1994). Contours are 40, 60, 80, 100 % of peak for both lines (I(C91α)=0.28 K km s^{-1}, I(C158μm)= $7.6{\cdot}10^{-4}$ erg/cm^2/sec/sr). The beamsizes of 60 and 82″ for the FIR and radio observations are indicated. The small squares show the positions observed in C91α.

[C II] 158 μm map of Jaffe et al. (1994) which is also shown in Fig. 3 (dashed lines). The [C II] 158 μm emission peaks slightly north of the radio emission peak. This is more easily seen in Fig. 4 where we show a north-south cut through the illuminating star HD 37903. From Gaussian fits, we find an offset of 50″ (0.1 pc) between the peaks of the radio and infrared line emission. The pointing uncertainty of the far-infrared measurements is 15″ and so we consider this offset significant.

3.2. C^{18}O *towards NGC 2023*

In Fig. 3.2, we show a comparison of our integrated C^{18}O (2-1) and (3-2) maps towards NGC 2023 with the contours of C91α

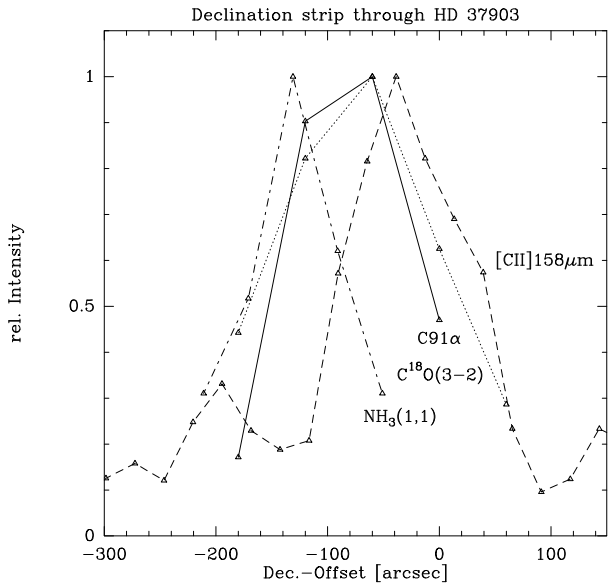

Fig. 4. Cross scans along $\alpha(1950) = 5^h39^m07^s.3$ through HD 37903. The ammonia data are taken from Miller (1984). The maximum intensities are 9.2 K km s^{-1}, 0.7 K km s^{-1} and $7.6 \cdot 10^{-4}$erg/cm^2/s/sr for the C^{18}O, radio and FIR observations, respectively.

emission. There is a general agreement between the two which is somewhat surprising at first glance because C91α is thought to form in the hot PDR layer closest to the exciting star whereas C^{18}O is presumably abundant in the cooler molecular region. From our data, the C^{18}O (3-2) maximum is at (6″, -66″) which is within pointing errors coincident with the C91α peak. The angular half-power width in declination which we derive from our C^{18}O (3-2) map is 172″ which becomes 155″ after deconvolving with an 75″ beam. The corresponding linear size is 0.31 pc.

It is interesting also that the line profiles observed in C^{18}O and C91α are similar which also argues for very close links between the two. We have examined our C^{18}O data for velocity shifts or gradients across the region mapped and find that the C^{18}O (3-2) velocity varies by at most 0.3 km s^{-1}. This puts a limit on any core rotation of 1.7 km s^{-1}/pc.

Our C^{17}O (2-1) and (3-2) observations have poor signal-to-noise ratio and we have therefore averaged the twelve positions measured (1..-1′,-3..0′) in both C^{18}O and C^{17}O. In this way, we determine the integrated intensity ratio C^{18}O(3-2)/C^{17}O(3-2) to be 4.8 ± 0.5 and the ratio C^{18}O(2-1)/C^{17}O(2-1) to be 3.1 ± 0.4.

In order to compare our C^{18}O (2-1) and (3-2) data, we have smoothed the (3-2) observations to a beam of 115 ″ and taken the ratio of the two maps. The integrated intensity ratio I(3-2)/I(2-1) along a north-south strip through HD 37903 is shown in Fig. 6 and a maximum in excitation is visible about 1′ south of HD 37903.

3.3. Comparison of C91α with molecular tracers in NGC 2023

In Fig. 4, we compare cuts in the FIR and radio carbon lines with observations in NH_3 (1,1) (Miller 1984) and C^{18}O (3-2). With our spatial resolution, the peak in C91α and C^{18}O coincides roughly with the arc of H_2 1-0 S(1) emission mapped by Gatley et al. (1987). This structure, which is also seen in CO(1-0) (Gatley et al.), probably represents the limb-brightened edge of a bubble blown by HD 37903. The C^{18}O emission may partly form in this region but clearly also originates in cooler material further from the star as evidenced by the ammonia emission (Fig. 4) which peaks 130″ to the south of HD 37903 and 50″ to the south of the peak in C91α. This suggests a picture in which ammonia, which is more sensitive to photodissociation than C^{18}O, is confined to dense clumps relatively far from the exciting star.

3.4. C91α towards S 140

In Fig. 2, we show our observed C91α spectra towards S 140 and in Table 1 we give the corresponding line parameters. We have clearly detected C91α emission both towards the infrared stars as well as towards the ionization front. This is of interest as previous carbon line detections in these regions were made with relatively large beams (e.g. Smirnov et al. 1995).

4. Physical parameters of the NGC 2023 PDR

The characteristics of the NGC 2023 PDR depend on physical parameters such as the density and UV field emitted by the star as well as on the geometry. They also depend on the gas phase abundances of critical elements such as oxygen and carbon. In this article, we have in general used solar abundances (i.e. C/H=$3.0 \cdot 10^{-4}$ and O/H=$5.0 \cdot 10^{-4}$ as in the Natta et al. study) but have also carried out some calculations using recent estimates for the "interstellar" abundances (see e.g. Mathis (1996), C/H = $1.4 \cdot 10^{-4}$ and O/H = $3.8 \cdot 10^{-4}$,the "Orion" value). The "interstellar" abundances may in fact be more relevant to NGC 2023 but for purposes of comparison with other models, the computations with solar values are useful. The PDR geometry relative to the observer and the exciting star can also play an important role. We discuss in this section face-on models where the star is assumed to be in the foreground relative to the PDR and edge-on models where star and gas are at the same distance from the sun.

We consider two main hypotheses while doing this. The first of these is that the carbon far infrared and radio lines are produced in the same region. With this assumption, we use the techniques discussed by Natta et al. (1994) to derive physical parameters for the region where carbon is singly ionized. This technique can be used as long as the PDR material is relatively homogeneous. However, there is evidence (e.g. Field et al. 1994) that the NGC 2023 PDR is highly clumped. Moreover, in such a clumpy medium, it seems probable that a situation will occur where the radio lines are emitted by the surfaces of the dense clumps whereas the [C II] 158 μm line (which has a critical density of $\sim$ 3000 cm^{-3}) comes at least in part from lower density inter-clump gas. In this case, a direct comparison

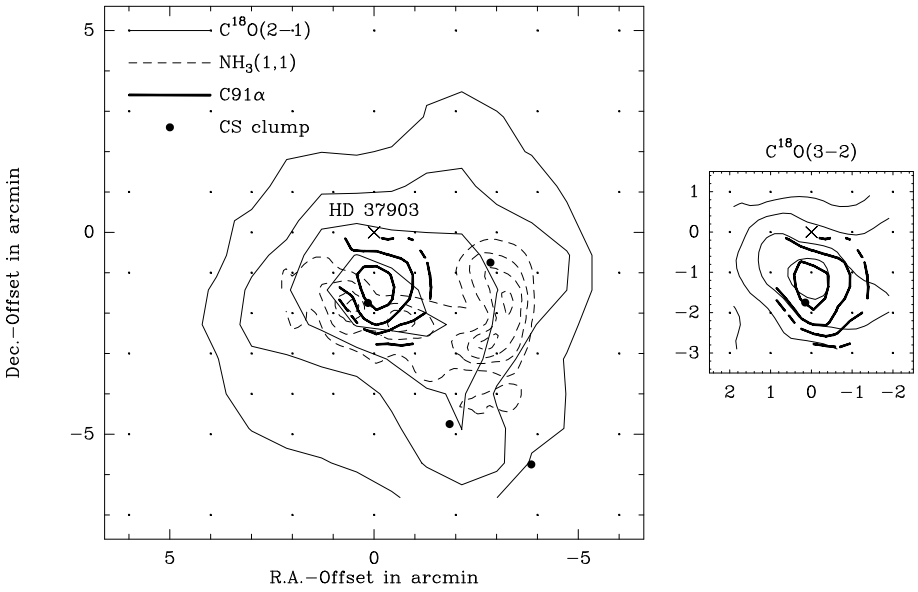

Fig. 5. $C^{18}O$ (2-1) (left panel) and (3-2) (right panel) in NGC 2023 (solid lines) in comparison with C91α (thick), NH_3 (1,1) (dashed, Miller 1984) and positions of CS clumps identified by Lada et al. (1991) shown as filled circles. Contours are 30, 50, 70, 90% of the peak values: $I(C^{18}O$ (2-1))=10.0 Kkm s^{-1}, $I(C^{18}O$ (3-2))=9.2 Kkm s^{-1}, I(C91α)=0.28 Kkm s^{-1}, $I(NH_3$ (1,1))=4.2 K.

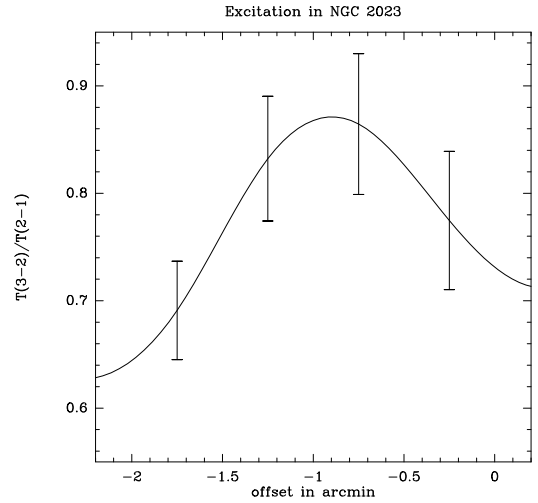

Fig. 6. $C^{18}O$ (3-2) and (2-1) integrated intensity ratio along a north-south strip through HD 37903.

of [C II] 158 μm and C91α may be misleading and the question arises of whether combining our radio data with observations of other PDR tracers is indeed useful. The [O I] 63 μm line with a critical density of $5 \cdot 10^5$ cm^{-3} (Tielens & Hollenbach 1985) seems a better candidate in this respect and thus we consider what constraints on the density and temperature of the NGC 2023 PDR clumps can be derived on the assumption that [O I] 63 μm and C91α form in the same layer. We discuss also the extent to which the recent models of Steiman-Cameron et al. (1996), who interpret their observations of a number of far infrared lines towards NGC 2023 in terms of a two-component model, need modification in the light of the radio recombination line data.

First however, we consider the homogeneous models and in particular the face-on case.

4.1. Face-on homogeneous PDR models

We use the technique devised by Natta et al. (1994) to derive the density and radiation field in the PDR region seen towards NGC 2023. In order to do this, we need to account for the differences in angular resolutions between the far IR (60″) and radio observations (82″) and we have therefore convolved the [C II] 158 μm map with a Gaussian of $\sqrt{82^2 - 60^2}$ ″ HPBW in order to reach the resolution of the radio observations.

The comparison of the observations with model results is shown in Fig. 7 (cf. Fig. 5 of Natta et al. 1994). We show (asterisks and open squares) the observed [C II] 158 μm and C91α intensities in S 140 and NGC 2023 compared with a grid of homogeneous isothermal models (dashed lines). We also have computed a small grid of homogeneous PDR models (filled triangles, Tielens & Hollenbach 1985) where density and incident FUV field G_0 are used as input parameters. G_0 is the FUV field measured in units of the equivalent Habing (1968) flux of $1.6 \cdot 10^{-3}$ ergs/cm^2/sec appropriate to the average interstellar medium.

Comparison of PDR model predictions with observations shows that the hydrogen number density varies from $5 \cdot 10^4$ cm^{-3} towards HD 37903 to 10^5 cm^{-3} at offset (0,-60) with the incident radiation field in both cases being of order 500 times the interstellar value. The temperature of an isothermal model consistent with the carbon line data is of order 100 K.

As a check on our results, we have selected the position (0,0), for which we determine from the two C lines a density of $3 \cdot 10^4$ cm^{-3} and a temperature of 125 K and calculated the [O I] 63 μm intensity for a simple isothermal model (see Sect. 4.3) with these parameters. We predict in this manner a [O I] 63 μm intensity of $3.5 \cdot 10^{-3}$ erg/cm^2/sec/sr roughly in agreement with the observed value (Steiman-Cameron et al. 1996) of $2 \cdot 10^{-3}$ erg/cm^2/sec/sr.

We note also that the FUV radiation field derived above ($G_0 \sim 500$) is an order of magnitude lower than that estimated

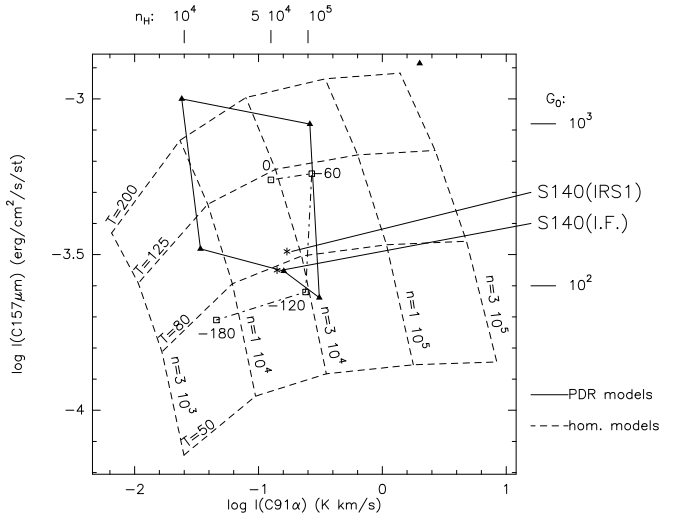

Fig. 7. Results of model calculations showing the Log of the FIR line intensity plotted against the Log of the integrated intensity of the [C II] 158 μm line. The dashed grid shows results for T=50, 80, 125, and 200 K and for hydrogen density between $3 \cdot 10^3$ and $3 \cdot 10^5$ cm^{-3}. The asterisks and the open squares are data points for S 140 (IRS 1 and ionization front) and NGC 2023 (the numbers denote the offsets from HD 37903) and the filled triangles are PDR model predictions based upon the results of Tielens & Hollenbach. Models are given for parameter pairs (G_0, n) where G_0 is the incident radiation field in units of the local value and n is the hydrogen density. No correction has been made for stimulated amplification of the radio lines.

by Steiman-Cameron et al. on the basis of the FIR dust continuum. In this case however (see Fig. 7), G_0 is mainly sensitive to [C II] 158 μm rather than to the radio line and the FIR continuum approach seems more direct. Moreover, as discussed below, use of interstellar rather than solar abundance for C causes the inferred G_0 to increase to values compatible with the FIR continuum estimate ($G_0 \sim 8000$). For comparison, the radiation field expected at a distance of 0.16 pc (80″ at the distance of NGC 2023 which is the observed offset of C91α from HD 37903) from a B1.5V star (see Draine & Bertoldi 1996) is about 2000 times the mean interstellar radiation field if one neglects dust extinction.

On the other hand, at the (0,-120″) offset, we estimate a density of 10^5 cm^{-3} but a radiation field of only 100 times the mean interstellar value. Thus, the density remains high at considerable distances from HD 37903. It seems likely that this reflects the properties of high density clumps within the molecular cloud.

4.2. Edge-on homogeneous models

The fluorescent molecular hydrogen emission observations of NGC 2023 by Gatley et al. (1987, see also Field et al. 1994) suggest an edge-on geometry for the PDR. This is further supported by the observed offset between radio and ammonia emission which can be qualitatively understood in an edge-on model in terms of the high photodissociation rate of NH_3 (see the models of Sternberg & Dalgarno 1995) which causes ammonia to be most abundant in heavily extincted regions far from the star. With this in mind, we have calculated models with edge-on geometry and a finite thickness d for the PDR.

In an edge-on scenario, the offset between FIR and radio lines could arise because of the different depths in the PDR from which the lines originate. The intensity of the C91α line, which is proportional to $T^{-1.5}$, increases with depth into the PDR and reaches a peak just in front of the transition zone C$^+$/CI/CO (Fig. 8). The [C II] 158 μm line on the other hand, has its maximum intensity closer to the surface of the PDR. PDR models show that this difference is of the order ΔA_v =1 largely independent of G_0 or n_H or equivalently a hydrogen column density of $2\,10^{21}$ cm^{-2}. The observed offset between FIR and radio lines (0.1 pc) then corresponds to a hydrogen density of $\simeq$ 7000 cm^{-3} which is comparable to the density estimates (10^4 cm^{-3}) derived on the basis of similar arguments from the observed size of the structure seen in vibrationally excited H_2 emission (Field et al. 1994).

There are however difficulties with this interpretation. The model shown in Fig. 8 ($n_{\rm H} = 10^4$ cm^{-3}, $G_0 = 100$) would lead to an offset between FIR and radio line of about 15″ but would need a PDR depth along the line of sight of 1.6 pc in order to explain the observed intensity of the radio line. Such an elongation along the line of sight seems highly unlikely (see discussion in Sect. 6) and we therefore reject this possibility. We conclude that a density gradient perpendicular to the line of sight is needed to explain the observations in the framework of an edge-on model. An alternative is a clumpy model as discussed in the next section.

4.3. Clumpy models

There are good reasons to expect PDRs to be clumped on size scales considerably lower than our effective linear resolution (see e.g. Tielens et al. 1993, Field et al. 1994). In the case of NGC 2023, Steiman-Cameron et al. (1996) have presented a two component model which accounts for their observations of the fine structure lines of [O I], [C II], and [Si II] as well as the available data for the mm-submm lines of CO. They conclude that the data are best fit by a model with warm (750 K) dense (10^5 cm^{-3}) clumps with a beam filling factor of 0.11 immersed in a cooler (250 K) halo of relatively low density (750 cm^{-3}). In this model, the [C II] 158 μm emission comes mainly from the low density extended medium, while the [O I], [Si II], and high level CO emission originates in the dense clumps. The observed offset between [C II] 158 μm and C91α then is caused by the fact that [C II] 158 μm is dominated by the low density gas in the central cavity around HD 37903 whereas C91α peaks up in the surrounding high density shell.

As shown by our homogeneous models discussed above, the low density extended component of Steiman-Cameron et al. contributes negligible to the observed C91α emission. Moreover, the high density component also fails (due to its low beam filling factor and high temperature) to account for the observed C91α flux (see Fig. 7). Finally, we note that these models have trouble accounting for the observed C91α linewidth (1.2

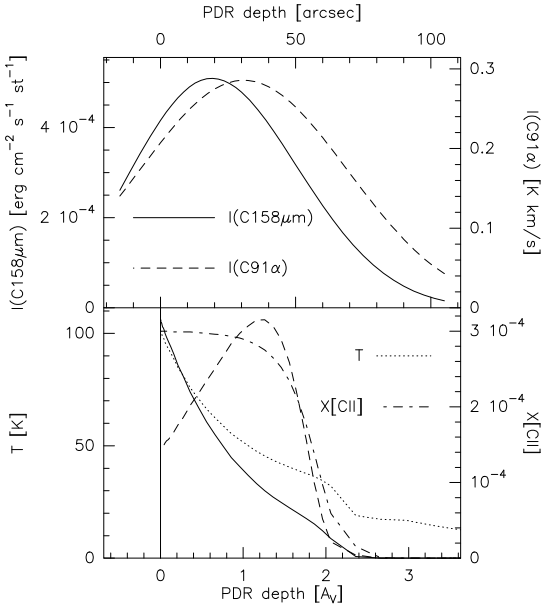

Fig. 8. The figures show a cut through a PDR in an edge-on model with G_0 = 100, n_H = 10^4 cm^{-3} and depth along the line of sight $d = 5 \cdot 10^{18}$ cm. The lower panel shows the intensities of radio and the FIR line as a function of PDR depth and the physical parameters T and X[C$^+$] from which the intensities are calculated. In the upper panel these intensities are folded with an 82 and 60″ beam, respectively.

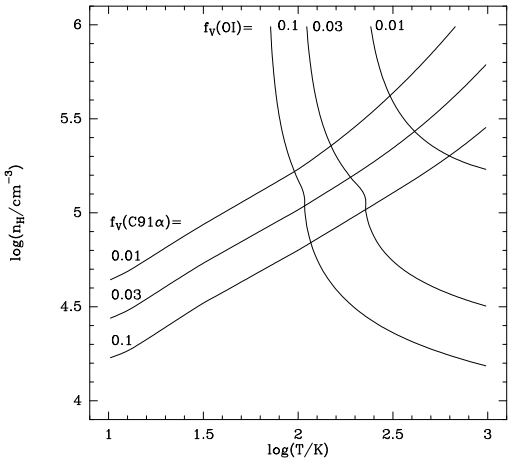

Fig. 9. Volume filling factor f_v required to account for the observed NGC 2023 C91α and [O I] 63 μm line intensities as a function of density and temperature in a clumpy model with depth along line of sight L=0.2 pc and clump radius r_c=0.02 pc. The observed C91α intensity is taken to be 0.2 Kkm s^{-1} and the observed [O I] 63 μm intensity to be $3.6 \cdot 10^{-3}$ erg/cm^2/sec/sr. Contours are shown in the density-temperature plane for f_v = 0.1, 0.03, and 0.01. Intersections of these curves for the same value of f_v allow one to deduce density-temperature combinations which explain both C91α and [O I] 63 μm.

km s^{-1}, see Table 1) which corresponds to an upper limit of 400 K on the kinetic temperature.

We now consider whether one can find two component models which account approximately for both the radio and FIR data. In such a clumpy model, it is clear that the carbon radio lines will form preferentially in the dense clumps (see discussion of Natta et al. 1994). The clumps will not make important contributions to the [C II] 158 μm emission unless their beam-filling factor is large but this is not necessarily the case for the [O I] 63 μm line with its much higher critical density. We therefore now discuss models where [O I] 63 μm and C91α form in the same region.

In particular, we have selected the observations at offset (30″,-30″) and analyzed a "clumpy model" for the emission of C91α and [O I] 63 μm (see Meixner & Tielens 1993 for a more general discussion of clumpy PDR models). We consider the emission in these two tracers from spherical clumps of radius r_c and volume filling factor f_v immersed in a cloud of size L. The beam-filling factor of the clumps is then $0.75Lf_v/r_c$. We suppose that the clumps are homogeneous with density $n_{\rm H}$ and temperature T and that carbon is singly ionized in a layer in which the hydrogen column density is $8 \cdot 10^{21}$ cm^{-2} (Tielens & Hollenbach 1985). With these assumptions, we compute the volume filling factor f_v required to account for the observed intensity in C91α (0.2 K km/s) and [O I] 63 μm towards NGC 2023 (see Steiman-Cameron et al. for a compilation of the OI data). In the case of C91α, f_v(C91α) is determined by an equation of the type,

$$I_\nu(\mathrm{C91}\alpha) = f_v(\mathrm{C91}\alpha) f_{em} j_\nu(\mathrm{C91}\alpha) \cdot L \qquad (1)$$

where f_{em} = 1 for $N_c = n_{\rm H} r_c < N_{cr} = 8 \cdot 10^{21}$ cm^{-2} and $f_{em} = 1 - (1 - r_{cr}/r_c)^3$ for $N_c > N_{cr}$ ($r_{cr} = N_{cr}/n_{\rm H}$). j_ν(C91α) is the C91α emissivity as given e.g. by Dupree & Goldberg (1970).

Fig. 9 shows contours of f_v(C91α) computed using Eq. 1 as a function of density and temperature. The calculations have been carried out for L=0.2 pc and r_c=0.02 pc. Since the C91α emissivity scales inversely with the gas temperature, warmer gas has to be denser (ie., higher emission measure) in order to explain the same observed intensity. Likewise, for the same gas temperature, a smaller volume/beam filling factor requires emission by denser gas. If one supposes the clumps to have beam-filling factors ($f_b = 7.5 f_v$) below unity, one requires densities above $2 \cdot 10^4$ cm^{-3} at 10 K and above $6 \cdot 10^4$ at 100 K in order to explain the observed C91α intensity.

One can carry out an analogous calculation for [O I] 63 μm where however there is the extra complication that in general the [O I] lines are optically thick and hence that the [O I] emissivity must be modified accordingly. Thus, one has :

$$I([\mathrm{O\ I}]\ 63\ \mu\mathrm{m}) = f_v(OI) f_{em} j([\mathrm{O\ I}]\ 63\ \mu\mathrm{m}) \beta(\tau_l) \cdot L \qquad (2)$$

where the escape probability (Hollenbach & McKee 1979, Eq. 5.10) $\beta(\tau_l)$ behaves roughly as $1/\tau_l$ for large line optical depth τ_l. The [O I] emissivity j([O I] 63 μm) can be computed using the expressions given, for example, by Tielens & Hollenbach (1991, Appendix B) and one thus can compute the filling factor $f_v(OI)$ required to explain the observed [O I] 63 μm intensity (I([O I] 63 μm)=$3.6 \cdot 10^{-3}$ erg/cm^2/sec/sr, Steiman-Cameron

et al. 1996). In this way, we have derived the loci of constant f_v given in Fig. 9.

The [O I] 63 μm emission from a clump in these models is usually optically thick. At high densities where the level populations are approximately thermalised, the line intensity thus depends only on temperature and beam (or volume) filling factor. This accounts for the rough density independence above 10^5 cm^{-3} shown by the [O I] 63 μm contours in Fig. 9.

Models which simultaneously fit both the [O I] 63 μm and C91α data require densities and temperatures in the range $7\cdot10^4$-$4\cdot10^5$ cm^{-3} and 100-300 K (consistent with the C91α line width), respectively. The volume filling factor varies correspondingly between 0.1 and 0.01. Thus, two component models with high density warm clumps (where C91α and [O I] 63 μm form) immersed in a low density medium ($n \sim 1000$ cm^{-3} which gives rise to [C II] 158 μm), can account for the observations. This model is in qualitative agreement with the results of Steiman-Cameron et al.. There is however an important difference: namely, we find that the clumps must be significantly cooler ($\sim$100-300 K vs. $\sim$750 K).

Our models of course are somewhat arbitrary (e.g. in the choice of r_c) but we think they provide a useful estimate of the physical conditions in the clump. They do not however attempt to fit other data such as the high-J CO lines which need to be understood in a more complete treatment of this problem. Understanding this will require treating the radiative transport in a manner analogous to that used for the homogeneous models of Sect. 4.1 .

4.4. Effect of "interstellar abundances" on inferred densities

As mentioned above, our results are sensitive to the assumed O and C abundances. We here briefly consider the nature of this dependence. The main effect is on the intensity of the C91α line which is proportional to the square of the gas phase carbon abundance (since n(C$^+$) is essentially equal to n_e). Thus overestimating the carbon abundance by a factor of 2 causes us to underestimate the hydrogen density required to account for the observations by a factor of 4. The analogous effect for the [C II] 158 μm line is merely linear and causes us to underestimate G_0.

We have attempted to assess the effect of changed abundances upon the models shown in Fig. 7. This suggests for example that one can fit our data at (0,-60) with a face-on model having $n_H = 7\cdot10^5$ cm^{-3} and $G_0 = 8000$. The FUV field is in better agreement with that obtained by Steiman-Cameron et al. using the FIR continuum data. The conclusion we draw from this is that the density estimates given in this section should probably be revised upwards roughly by a factor of 4.

5. Density and UV field in S 140

Using the [C II] 158 μm intensity towards S 140 observed by Schneider et al. (1995) together with our radio measurements, we derive from the models in Fig. 7 a density of about $5\cdot10^4$ cm^{-3} and an incident FUV field of $G_0 \approx 100-200$. The FUV field towards IRS 1 is slightly higher than towards the ionization front. If the B0 star HD 211880 were to be the only source of FUV flux, G_0 would decrease from 150 at the ionization front (Keene et al. 1985) to 100 at the position of the embedded infrared sources. It is possible however that one of the embedded stars contributes to the FUV flux.

6. Characteristics of the molecular core in NGC 2023

We consider in this section the characteristics of the molecular core in NGC 2023 which we can derive from our C^{18}O observations.

Our measurements of C^{18}O (2-1) and C^{18}O (3-2) allow us to place important constraints on the molecular gas associated with the NGC 2023 PDR. When analyzing these data, we will make two assumptions which we now discuss briefly. The first is that the basic density structure (i.e. density and volume filling factor) of the molecular gas and of the PDR is the same. Thus in a homogeneous model, the density in the region responsible for C^{18}O emission and that in the layer responsible for C91α emission are identical. They differ in the degree of penetration of the UV field and consequently in the temperature. This assumption is justified by the general agreement in spatial and velocity distributions of C^{18}O and C91α (see Fig. 3.2) but it is certainly debatable.

A second assumption is that the molecular/PDR region seen towards NGC 2023 is not greatly elongated along the line of sight. Molecular cores are often elongated but an aspect ratio of more than 2 is unusual (Myers et al. 1991) and we thus conclude that the depth of the C^{18}O emitting region in the line of sight direction is less than 0.6 pc (or twice the value estimated as the half-power diameter in Sect. 3.2). Again the assumption is questionable but it seems a reasonable starting hypothesis. It would incidentally invalidate some of the more extreme edge-on models discussed in Sect. 4.2.

With these two assumptions in mind, we now consider the significance of our observed C^{18}O(3-2)/C^{18}O(2-1) ratio (see Fig. 6). Our C^{17}O results (see Sect. 2.2) show that C^{18}O is close to being optically thin in NGC 2023 and from the observed C^{18}O(3-2)/C^{17}O(3-2) integrated intensity ratio, we estimate the C^{18}O(3-2) optical depth is at most 0.5 (the interstellar C^{18}O/C^{17}O abundance ratio is estimated to be 3.2 ± 0.2 in the local ISM (Wilson & Rood 1994). Alternatively, we used the ^{13}CO intensities measured by Kramer et al. (1996, see also Kramer 1992) together with an interstellar ^{13}CO/C^{18}O ratio of 7.3 (estimated from the local ISM ^{16}O/^{18}O and ^{12}C/^{13}C ratios given by Wilson & Rood) to estimate the optical depth in the C^{18}O lines and found τ(2-1)=0.45 ± 0.05 and τ(3-2)=0.4 ± 0.05.

In view of this, it seems reasonable as a first estimate to use the usual (low optical depth LTE) formula to calculate the C^{18}O column densities and the molecular rotation temperature. We find $T_{\rm rot}$=13 ± 3 K and N(C^{18}O) = $(4\pm1)\cdot10^{15}$ cm^{-2} which for C^{18}O/H$_2$= $2.3\cdot10^{-7}$ (Lada et al 1994) corresponds to N(H$_2$) = $1.7\cdot10^{22}$ cm^{-2}. This corresponds to a visual extinction of approximately 18 magnitudes and (using the assumption

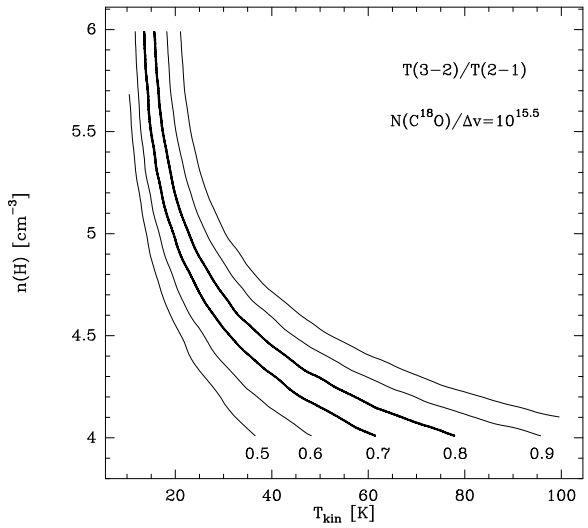

Fig. 10. Predictions of the $C^{18}O$(3-2)/(2-1) line ratio for $N(C^{18}O)/\Delta v = 10^{15.5}$ cm^{-2}/km s^{-1}using a statistical equilibrium model. The range of observed values are indicated by thick contours.

about the depth of the molecular core along the line of sight mentioned earlier), the H_2 density must be at least 10^4 cm^{-3}.

With this in mind, we have carried out statistical equilibrium calculations aimed at predicting the $C^{18}O$(3-2)/$C^{18}O$(2-1) intensity ratio as a function of density and temperature. We have used here an LVG approach to estimate the line escape probability for a $C^{18}O$ column density to line width ratio of $10^{15.5}$ cm^{-2}/(km s^{-1}) which corresponds roughly to the LTE estimate given above. However, given that the $C^{18}O$ lines are optically thin, this assumption does not greatly influence the results. More critical are the collisional rates for which we have used the results of Flower & Launay (1985). The results, displayed in Fig. 10, show the predicted ratio of $C^{18}O$(3-2)/(2-1) as a function of density and temperature. One sees that the kinematic temperature is constrained to the range 13-80 K. This is consistent with the results of Jaffe et al. (1990) who observed $C^{18}O$(2-1) with a 32″ beam and found a main-beam brightness temperature of 11.8 K 100″ SE of HD 37903. Below 20 K, densities of above 10^5 cm^{-3} are implied by the observations and under these conditions, the lower levels of $C^{18}O$ are close to being thermalised. At higher temperatures, lower densities are possible and at 80 K (Jaffe et al. 1990, Jansen et al. 1993 based upon CO data), the density may be as low as 10^4 cm^{-3}. There is probably a great range of temperatures in the molecular core seen in $C^{18}O$. Walmsley & Ungerechts (1983) estimated temperatures of order 15-20 K at three positions in NGC 2023 on the basis of their ammonia data and it is likely that the ^{12}CO observations may sample a surface layer similar to that observed in CN (Fuente et al. 1995).

On this basis, we conclude that the total hydrogen density in the molecular core is at least 10^4 cm^{-3} and most probably above 10^5 cm^{-3}. This is consistent with estimates made by Fuente et al. (1995). It should be compared with the values estimated in Sect. 4 for the hydrogen density in the region responsible for C91α and [C II] 158 μm emission. Our estimates for the density in the molecular core are consistent with those derived for the homogeneous face-on model of Sect. 4.1.

The above results allow us to determine the mass and overall properties of the molecular core observed in $C^{18}O$. We determine a mass of 30 $M_\odot$ by integrating our observed $C^{18}O$ column density over the molecular core. The turbulent kinetic energy in the cloud (see Harju et al. 1993) is $4 \cdot 10^{44}$ ergs and the gravitational energy (for spherical geometry) $3 \cdot 10^{44}$ ergs. Thus to within geometrical uncertainties, the molecular cloud is virialised.

7. Discussion and conclusion

The main conclusion from this work is that a large fraction of the gas seen towards NGC 2023 is at densities above 10^5 cm^{-3}. Put in other terms, the beam filling factor of such high density gas cannot be much less than unity. This is true both for the ionized atomic gas which emits carbon radio recombination lines and the molecular component seen in $C^{18}O$ emission. We estimate that there are 30 $M_\odot$ of molecular gas in the molecular core associated with NGC 2023 corresponding to about 20 magnitudes of visual extinction. The amount of partially ionized gas is probably a factor of 2 lower. It seems likely that the densities in the molecular and partially ionized layers are similar although the temperatures differ by 1-2 orders of magnitude. Verification of this using other density tracers would be useful.

It is worth noting that various other tracers besides the CI radio recombination lines and OI fine structure lines indicate the presence of high densities in the NGC 2023 PDR. First, the observed H_2 S(1)1-0/2-1 line ratio 80″ south of HD 37903 indicates partial thermalisation of the v=1 level. The inferred densities are somewhat controversial due to uncertainty in the collision rates and range from 10^4 to 10^5 cm^{-3} with the most reliable estimates at the high end of the range (Black and van Dishoeck 1987, Sternberg and Dalgarno 1989, Burton et al. 1990, Draine and Bertoldi 1996). The spatial structure of the H_2 emission (Gatley et al. 1987 , Field et al. 1994) indicates the presence of a dense shell with a filling factor which is probably too small to account for the C91α observations. On the other hand, the intense CO(7-6) emission observed by Jaffe et al. (1990) also indicates the presence of a warm dense component (10^5 cm^{-3}) with beam filling factor of order unity.

Our data do not have sufficient angular resolution to make definitive statements concerning the geometry or structure of the PDRs seen towards NGC 2023 and S 140. Nevertheless, they show that combining the radio lines with other PDR tracers can allow useful limits to be placed on the physical parameters of the high density clumps. In particular, using [O I] 63 μm in combination with the radio lines has allowed us to estimate densities upward of 10^5 cm^{-3} and temperatures of order 200 K in the region where carbon is ionized.

Acknowledgements. We thank D. Jaffe for supplying us with numerical data from the [C II] 158 μm observations of Orion B. The KOSMA 3m telescope is operated by the University of Cologne and supported by the Deutsche Forschungsgemeinschaft through grant SFB 301, as

well as special funding from the Land Nordrhein-Westfalen. The Observatory is administered by the Internationale Stiftung Hochalpine Forschungsstationen Jungfraujoch und Gornergrat, Bern.

References

Anthony-Twarog B.J. 1982, AJ 87, 1213
Black J.H., van Dishoeck E.F. 1987, ApJ, 322, 412
Blair G.N., Evans N.J. II, Vanden Bout P.A., Peters W.L. 1978, ApJ 219, 896
Boreiko R.T., Betz A.L., Zmuidzinas J. 1990, ApJ 353, 181
Burton M.M., Hollenbach D.J., Tielens A.G.G.M. 1990, ApJ, 365, 620
Burton M.G., Bulmer M., Moorhouse A., Geballe T.R., Brand P.W.J.L. 1992 Mon. Not. RAS, 257, 1P
Draine B.T., Bertoldi F. 1996, ApJ, 468, 269
Dupree A., Goldberg L. 1970, ARAA 8, 231
Field D., et al. 1994, A&A 286, 909
Flower D.R., Launay J.M. 1985 Mon. Not. RAS, 214, 271
Fuente A., Martin-Pintado J., Gaume R. 1995, ApJ 442, L33
Gatley I. et al. 1987, ApJ 318, L73
Genzel R. 1992 , in "The galactic Interstellar Medium", p275, (Burton W.B., Elmegreen B.G., Genzel R.), Springer
Grossman E. 1989,"AT - Atmospheric Transmission Software, User's Manual", Univ. of Texas, Austin
Habing H.J. 1968, Bull. Astr. Inst. Netherlands, 19,421
Harju J., Walmsley C.M., Wouterloot J.G.A. 1993, A&AS 98, 51
Harvey P.M., Thronson H.A., Gatley I. 1980, ApJ 235, 894
Hernichel J., Krause D., Röhrig R., Stutzki J., Winnewisser G. 1992, A&A 259, L77
Hollenbach D., McKee C.F. 1979, ApJS 41, 555
Hollenbach D., Takahashi T., Tielens A. 1991, ApJ 377, 192
Howe J.E., Jaffe D.T., Genzel R., Stacey G.J. 1991, ApJ 373, 158
Jaffe D.T., Genzel R., Harris A.I., Howe J.E., Stacey G.J., Stutzki J., 1990, ApJ 353, 193
Jaffe D.T., et al. 1994 ApJ 436, 203
Jansen D.J., van Dishoeck E.F., Black J.H. 1994 A&A 282, 605
Keene J., Blake G.A., Phillips T.G., Huggins P.J., Beichman C.A. 1985 ApJ 299, 967
Knapp G.R., Brown R.L., Kuiper T.B.H. 1975, ApJ 196, 167
Knapp G.R., Brown R.L., Kuiper T.B.H., Kakar R.K. ApJ 204, 781
Kramer C. 1992, PhD. thesis, Univ. of Cologne
Kramer C., Stutzki J., Winnewisser G. 1996, A&A 307, 915
Lada C.J., Lada E.A., Clemens D.P., Bally J. 1994, ApJ 429, 694
Lada E.A., De Poy D.L., Evans N.J. II, Gatley I. 1991, ApJ 371, 171
Mathis J.S. 1996, ApJ 472, 643
Meixner M., Tielens A. 1993, ApJ 405, 216
Miller M. 1984, Doktorarbeit, University of Cologne
Myers P.C., Fuller G.A., Goodman A.A., Benson P.J. 1991, ApJ 376, 561
Natta A., Walmsley C.M., Tielens A. 1994, ApJ 428, 209
Pankonin V., Walmsley M. 1976, A&A 48, 341
Pankonin V., Walmsley C.M. 1978, A&A 67, 129
Schneider N. et al. 1995, "Large Scale Submm-CO and FIR [CII] observations of the Rosette Molecular Complex and S140/L1204", Proceedings of the 2nd Cologne-Zermatt Symposium, Winnewisser G., Pelz G.(Ed.)
Sellgren K., Werner M.W., Dinerstein H.L. 1992, ApJ 400, 238
Smirnov G.T., Sorochenko R.L., Walmsley C.M., 1995, A&A 300, 923
Stacey G.J. et al. : 1993 , ApJ 404, 219
Steiman-Cameron T.Y., Haas M.R., Tielens A., Burton M. 1996, ApJ, in press
Sternberg A., Dalgarno A. 1989, ApJ, 347, 863
Sternberg A., Dalgarno A. 1995 , ApJS 99, 565
Tielens A. , Hollenbach D. : 1985 , ApJ 291, 722
Tielens, A.A.G.M., Meixner, M.M., van der Werf, P.P., Bregman, J., Tauber, J.A., Stutzki,J., Rank, D. 1993, Sci 262,86
Ungerechts H., Walmsley C.M., Winnewisser G. 1986, A&A 157, 207
Walmsley C.M., Ungerechts H. 1983, A&A 122, 164
Wilson T.L., Rood R.T. 1994, ARAA, 32, 191
Winnewisser G., Zimmermann P., Hernichel J.,Miller M., Schieder R. 1990, A&A 230, 248
Witt A.N., Schild R.E., Kraiman J.E. 1984, ApJ, 281, 708
Wyrowski F. 1994 , Diplomarbeit, University of Bonn
Zhou S., Evans N.J., Mundy L.G., Kutner M.L. 1993, ApJ 417, 613
Zhou S., Butner H.M., Evans N.J. II, Güsten R., Kutner M.L., Mundy L.G. 1995 ApJ 428, 219

This article was processed by the author using Springer-Verlag LaTeX A&A style file *L-AA* version 3.